Lab on a Chip

PAPER

View Article Online
View Journal | View Issue

Cite this: *Lab Chip*, 2015, **15**, 2419

Differentiation of neuroepithelial stem cells into functional dopaminergic neurons in 3D microfluidic cell culture†

Edinson Lucumi Moreno,[a] Siham Hachi,[a] Kathrin Hemmer,[a] Sebastiaan J. Trietsch,[b] Aidos S. Baumuratov,[a] Thomas Hankemeier,[bc] Paul Vulto,[bc] Jens C. Schwamborn[a] and Ronan M. T. Fleming*[a]

Received 12th February 2015,
Accepted 30th March 2015

DOI: 10.1039/c5lc00180c

www.rsc.org/loc

A hallmark of Parkinson's disease is the progressive loss of nigrostriatal dopaminergic neurons. We derived human neuroepithelial cells from induced pluripotent stem cells and successfully differentiated them into dopaminergic neurons within phase-guided, three-dimensional microfluidic cell culture bioreactors. After 30 days of differentiation within the microfluidic bioreactors, *in situ* morphological, immunocytochemical and calcium imaging confirmed the presence of dopaminergic neurons that were spontaneously electrophysiologically active, a characteristic feature of nigrostriatal dopaminergic neurons *in vivo*. Differentiation was as efficient as in macroscopic culture, with up to 19% of differentiated neurons immunoreactive for tyrosine hydroxylase, the penultimate enzyme in the synthesis of dopamine. This new microfluidic cell culture model integrates the latest innovations in developmental biology and microfluidic cell culture to generate a biologically realistic and economically efficient route to personalised drug discovery for Parkinson's disease.

Introduction

Although our understanding of aetiopathogenesis of neurodegeneration has rapidly developed in the past two decades, this has not yet been translated into any neuroprotective treatment. The aetiological diversity of neurodegenerative diseases and the estrangement of existing preclinical models from clinical diseases are critical issues being addressed within personalised biomedicine. Deriving cells with neuronal phenotypes from patients with neurodegenerative disorders through cellular reprogramming has the potential to revolutionise preclinical disease modelling.[1] Human terminally differentiated cells can be reprogrammed to an embryonic-like state through the ectopic expression of only four stem cell transcription factors.[2,3] The resulting induced pluripotent stem cells (iPSCs) offer a new tool for *in vitro* disease modelling,[4] especially relevant for neurodegenerative diseases as access to human neuronal cells is otherwise difficult. However, developing *in vitro* cellular models to study neurodegenerative diseases requires the use of appropriate neuronal cell types under the right biological, chemical and physical conditions.[5–7] Efficient neural induction of iPSCs can be achieved by inhibiting the transforming growth factor beta and bone morphogenetic protein signalling pathways.[8] A combinatorial activation of the antagonising neural plate border pathways WNT and SHH enables the generation and long-term renewal of these cells.

A key pathological feature of Parkinson's disease is the progressive loss of nigrostriatal dopaminergic neurons (DNs).[9] Starting with fibroblasts obtained from familial or sporadic Parkinson's disease patients, dysfunctional cellular phenotypes are observed in macroscopic *in vitro* cultures of iPSC-derived DNs,[10–13] opening up the possibility of screening for compounds that rescue dysfunctional cellular phenotypes.[12] The aforementioned personalised *in vitro* disease models are based on macroscopic, two dimensional cultures. Macroscopic culture in this context refers to the use of macroscopic-scale cell culture devices (Petri dishes, flasks and multi-well plates). Two dimensional culture cannot reproduce the normal anatomy and physiology of cells designed to live in a three dimensional microenvironment.[14] Moreover, macroscopic culture is inefficient with respect to the use of scarce patient derived cellular materials and expensive reagents. Medium requirements in such devices range from 20 mL for large flasks to 200 μL for each well of a 96-well plate,[15,16] requiring the use of proportionate amounts of growth factors.

Reinhardt *et al.* recently established a protocol, using only small molecules, for derivation and expansion of human

[a] *Luxembourg Centre for Systems Biomedicine, University of Luxembourg, 7 avenue des Hauts-Fourneaux, L-4362 Esch-sur-Alzette, Luxembourg. E-mail: ronan.mt.fleming@gmail.com*
[b] *Mimetas B.V, PO Box 11002, 2301EA Leiden, The Netherlands*
[c] *Analytical BioSciences Division, Leiden Academic Centre for Drug Research, Leiden University, Einsteinweg 55, 2333CC Leiden, The Netherlands*

† Electronic supplementary information (ESI) available: Supplementary movies 1–3. See DOI: 10.1039/c5lc00180c

neuroepithelial stem cells from human induced pluripotent stem cells or human embryonic stem cells.[13] Using additional growth factors, these neuroepithelial stem cells can be differentiated into neural tube and neural crest lineages, including midbrain-specific DNs that are electrophysiologically functional and integrate after transplantation into the midbrain of adult mice.[13] Reinhardt *et al.*'s protocol is well suited for large-scale *in vitro* disease modelling and phenotypic screening as it robustly generates a large and immortal population of neuroepithelial stem cells, obviating the requirement for costly growth factors or cumbersome manual steps. Nevertheless, the subsequent differentiation step does require costly growth factors and to date, it has only been completed in two dimensional macroscopic cell culture[13] following transplantation in the brain of mice.[17–19] Human dopaminergic neurons derived from neural progenitor cells have been macroscopically cultured in 3D neurospheres,[20,21] but to our knowledge, 3D microfluidic cell culture of iPSC-derived dopaminergic neurons has not yet been reported.

Microfluidic cell culture offers a complementary approach to study neuronal differentiation from induced pluripotent stem cells under controlled experimental conditions.[22] 3D microfluidic cell culture devices permit spatio-temporal control over the cellular microenvironment, monitoring of cellular events using current microscopy techniques and perfusion culture to exchange nutrients, growth factors, signalling molecules, waste products and gasses at controlled rates.[23–25] Microfluidic cell culture comes with many advantages and challenges, determined by the quality of the match between the microfluidic cell culture device and the cell culture phenotype desired.[16] Biocompatibility aside, any macroscopic cell culture protocol is the result of heuristic optimisation by generations of biologists and cannot be assumed to be optimal for microfluidic cell culture as the mechanisms of fluid and gas exchange in a microfluidic device will deviate from the exchange typical for macroscopic culture.[16]

Trietsch *et al.* recently described a stratified 3D cell culture bioreactor.[26] Each bioreactor contains a lane of hydrogel-embedded cells and one or more adjacent lanes of laminarly flowing liquid. Every pair of lanes is partially separated by a phaseguide, which is a geometric feature introduced to pattern liquids flowing into each bioreactor. Each phaseguide induces a meniscus pinning effect that forces an advancing liquid to align itself with the phaseguide instead of flowing over it.[27,28] To load a bioreactor, cells are mixed with a liquified, surrogate extracellular matrix that is then dispensed into a well connected to a phaseguide delimited lane. Upon gelation this lane becomes the aforementioned lane of gel-embedded cells. Next, fresh medium is added to another well that is connected to a medium lane adjacent to the gel-embedded cells.

In a typical bioreactor,[26] a phaseguide is not higher than one fourth of the height of a lane, permitting diffusion between the lane of gel-embedded cells and the fluid medium lane(s). While diffusion will allow the supply of nutrients and efflux of waste metabolites, cells embedded within the gel are shielded from shear stress. Arrays of bioreactors are incorporated in a microtiter plate format, termed as OrganoPlate (Mimetas BV, Leiden), which is fully compatible with standard laboratory automation equipment. The functionality of this platform with respect to 3D culture of immortalised cell lines with continuous perfusion, co-culture and invasion has already been established,[26] but not yet for differentiation of induced pluripotent stem cell-derived cell lines.

Hydrogels are often used as a surrogate extracellular matrix for 3D culture because of their biomechanical properties. They provide mechanical integrity, yet permit the diffusion of signalling molecules, nutrients and metabolic wastes.[29] Natural hydrogels, *e.g.*, Matrigel, fibrin gel or alginate gel, are composed of proteins and extracellular matrix components[30] that provide a suitable extracellular matrix environment for 3D cell culture and endogenous factors that promote proliferation and development. Synthetic hydrogels like poly(ethylene glycol), poly(vinyl alcohol) and poly(2-hydroxy ethyl methacrylate) act as a template for cell culture, but they lack endogenous factors.[29,30] A combination of natural and synthetic polymers, *e.g.*, poly(ethylene glycol) and collagen, can be used as a cell entrapping material.[29] A commonly used natural hydrogel is BD Matrigel, a reconstituted basement membrane preparation extracted from the Engelbreth–Holm–Swarm (EHS) mouse sarcoma, a tumour rich in extracellular matrix proteins. Matrigel is composed of 60% laminin, 30% type IV collagen and 8% entactin, in addition to growth factors and other molecules. Entactin acts as a bridging molecule that interacts with laminin and collagen IV contributing to the structural organisation of Matrigel as an extracellular matrix. The interaction of cells in culture with the surrounding extracellular matrix is an active process. Cultured cells may respond to their local environment remodelling the extracellular matrix by synthesising a new extracellular matrix or degrading it by the action of extracellular enzymes.[31]

In this paper, we report the successful integration of advanced developmental cell biology and microfluidic cell culture technology. We efficiently differentiated human iPSC-derived neuroepithelial stem cells[13] into functional DNs within phase-guided 3D cell culture bioreactors.[26] After 30 days in culture, we confirmed known phenotypic characteristics of DNs by calcium imaging and immunofluorescence. 3D image analysis revealed mature neurons that possessed long neurites showing an interconnected neuronal population. This paper establishes that phase-guided 3D cell culture bioreactors can be successfully integrated with cellular reprogramming of neuroepithelial stem cells to produce an *in vitro* dopaminergic neuronal cell culture model. This model is robust, cost efficient, physiologically proximal and ready for parallelism by laboratory automation and personalisation by supply of patient derived iPSCs from dedicated bio-banks.

Materials and methods

Microfluidic device

Cells were cultured in 2-lane and 3-lane *OrganoPlates* (Mimetas BV, Leiden, The Netherlands) consisting of arrays

of microfluidic bioreactors in a microtiter plate format, detailed previously[26] (Fig. 1). In brief, a 2-lane OrganoPlate consists of an array of 96 bioreactors. Each culture chamber is juxtaposed to 4 wells of a 384 well plate with one *gel inlet well* (Fig. 1b, 1) for loading gel-embedded cells into the culture lane and one *readout window* (Fig. 1b, 3) for monitoring the culture lane by inverted light microscopy. In addition, each bioreactor has a *perfusion inlet well* (Fig. 1b, 2) connected to a *perfusion outlet well* (Fig. 1b, 4) *via* a medium perfusion lane, where the flow of fluid is driven by gravity. In each culture chamber, during cell loading a *phaseguide* prevents liquefied gel-embedded cells from leaving the culture lane and entering the medium lane (Fig. 1c–e). A phaseguide is a patterned pinning barrier that controls the liquid–air interface by forcing it to align with the ridge and therefore allowing the filling of microfluidic structures[27] (ESI† movie 1). 2- and 3-lane OrganoPlates are the same, except that the latter consists of an array of 40 bioreactors, each of which contains one culture chamber, composed of three lanes separated by two phaseguides (Fig. 1f–h). This gives more options for stratified culture as only one lane must be used for medium perfusion and only one culture lane must be used for gel-embedded cells, the third can be used for either purpose.

Human neuroepithelial stem cell culture

Human neuroepithelial stem cells (hNESCs) derived from iPSCs were maintained and differentiated into DNs by adapting an existing protocol described in detail by Reinhardt *et al.*[13] We summarise this protocol and highlight any adaption for microfluidic cell culture. Small molecules (ascorbic acid, CHIR, PMA and dbcAMP) and specific growth factors (BDNF, GDNF and TGFβ3) are used to differentiate hNESCs into midbrain specific DNs. The culture preparation medium *N2B27 medium* consisted of equal amounts of neurobasal medium (Life Technologies) and DMEM/F12 medium (Life Technologies) supplemented with 1% penicillin/streptomycin (Life Technologies), 2 mM L-glutamine (Life Technologies), 1 : 100 B27 supplement without vitamin A (Life Technologies) and 1 : 200 N2 supplement (Life Technologies). hNESCs were maintained and proliferated in N2B27 medium up to 70% confluence to have enough cell material to load into the wells of the OrganoPlate.

Dopaminergic neuronal differentiation

The *maintenance medium* used to maintain the hNESCs in culture consisted of N2B27 medium with 0.5 μM PMA (Enzo Life Sciences), 3 μM CHIR (Axon Medchem) and 150 μM ascorbic acid (Sigma Aldrich). This medium was used to prepare the hNESCs at an average cell density of 7 million cells per ml. Corning Matrigel hESC-qualified matrix catalogue number 354277, lot number 3318549 (Discovery Labware) at 50% from the reconstituted stock, with the cell suspension in maintenance medium, was used as the extracellular matrix. hNESCs in the maintenance medium were mixed with an equal amount of Matrigel and 1 μL of this mixture was loaded into each inlet wells of the 2-lane (2 μL in the 3-lane) microfluidic bioreactors in an OrganoPlate, using a repeating pipette (Eppendorf) following the plate loading protocol

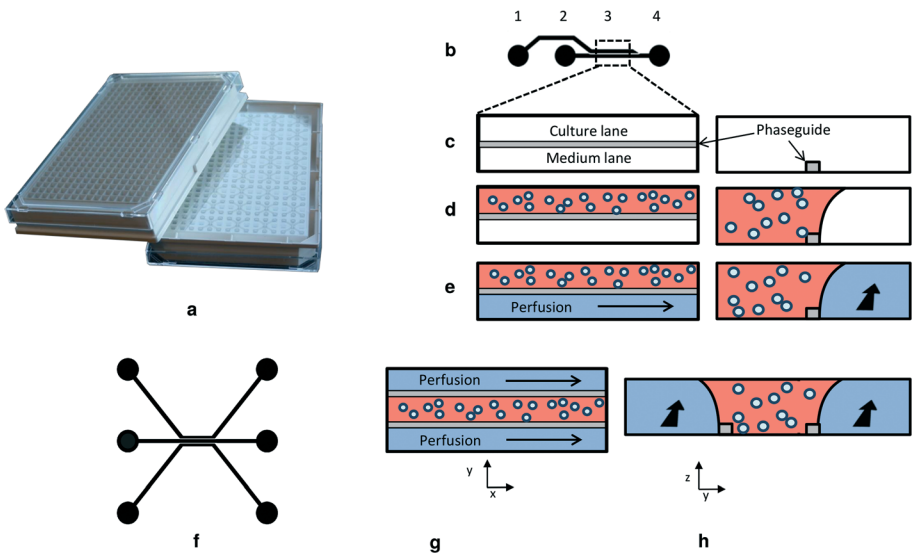

Fig. 1 OrganoPlate concept and filling procedure: (a) top and bottom views of a 3-lane OrganoPlate. The top is based on a 384-well microtiter plate format, while the bottom consists of 40 microfluidic bioreactors each with one culture chamber. (b) Scheme of a single 2-lane bioreactor composed of a gel inlet (1), a perfusion inlet (2), an optical readout window (3) and a perfusion outlet (4). (c) A horizontal view of the readout window and its cross section. The 2-lane culture chamber is separated by a phaseguide to allow selective gel patterning. (d) Cells are loaded within the liquefied gel and selectively patterned in the culture lane by the phaseguide. (e) Upon gelation, the medium is introduced in the perfusion lane and perfusion is driven by gravitational leveling between the perfusion inlet well and the perfusion outlet well. (f) 3-lane bioreactor consisting of two perfusion lanes and one culture lane; (g) gel-embedded cells are perfused from two sides; (h) vertical cross sectional view of (g).

previously described by Trietsch *et al.*[26] In each microfluidic bioreactor, the hNESCs are embedded within the Matrigel adjacent to one or more perfusion lanes, rather than seeded on top of the Matrigel with media above, as in the macroscopic culture protocol reported by Reinhardt *et al.*[13] After loading the cells into the culture chambers of the OrganoPlate, the plate was incubated at 37 °C and 5% CO_2 for 10 min to allow initial gelation of the Matrigel. To start medium perfusion by gravity, the maintenance medium was added to the perfusion inlet and outlet wells where an average fluid flow of 1.5 μL h^{-1} is achieved.[26]

The *differentiation medium with PMA* used to induce the differentiation of hNESCs towards DNs consisted of N2B27 medium with 200 μM ascorbic acid, 0.01 ng μL^{-1} BDNF (Peprotech), 0.01 ng μL^{-1} GDNF (Peprotech), 0.001 ng μL^{-1} TGFβ3 (Peprotech), 2.5 μM dbcAMP (Sigma Aldrich) and 1 μM PMA. The differentiation medium with PMA was changed every 2 days during the first 6 days of culture in the differentiation process.

For the maturation of differentiated neurons, PMA was no longer added to the differentiation medium, *differentiation medium without PMA*, from day 7 onwards; this differentiation medium without PMA was changed every 2 days for 3 weeks. Exchange of the differentiation medium with and without PMA was done 3 times a week to ensure the stability of the small molecules used during the differentiation process.

To monitor cellular morphology during differentiation, bright field images were acquired using a Zeiss Axiovert 40 CFL microscope equipped with a cooled CCD camera (Zeiss AxioCam Mrm, Zeiss).

Calcium imaging

A calcium imaging assay was performed on representative wells. 80 μL of 5 μM cell permeant Fluo-4 AM (Life Technologies) in neurobasal medium was added to inlet wells of microfluidic bioreactors at room temperature. Fluorescence images were acquired using an epifluorescence microscope (Leica DMI6000B) equipped with a cooled sCMOS camera (Neo 5.5, Andor Technology) with both apparatus controlled with Micro-manager (version 1.4).[32] Images were sampled at a rate of 8.4 Hz for ~2 min, stored as image stacks and analysed using custom Matlab (version 2013b; MathWorks) scripts. Fluorescence traces were extracted from manually segmented regions of interest corresponding to neuronal cell bodies and were presented as relative changes in fluorescence ($\Delta F/F$). Thereafter, the most probable spike train was inferred from fluorescence observations using a fast non-negative deconvolution algorithm described by Vogelstein *et al.*[33] The output of this algorithm is the probability that a spike occurred in a given time frame. In order to binarise the resulting spike train (1 for neuron activated and 0 for neuron not activated), we thresholded the vector of probabilities v such that the spikes with a probability below 2/3 ($\min(v)$ + $\max(v)$) were set to 0 and the remaining ones were set to 1. Thus, spikes with the highest probabilities indicated the activation of the neuron.

Immunofluorescence staining

The *in vitro* dopaminergic phenotype is characterised by the expression of specific neuronal markers, TUBβIII and tyrosine hydroxylase (TH), the rate limiting enzyme in the biosynthesis of dopamine.[13,34,35] Immunostaining for TH positive cells was performed on representative wells at day 30 of differentiation. Differentiated cells were fixed with 4% paraformaldehyde (PFA) in 1× phosphate-buffered saline (PBS) for 15 min, followed by permeabilisation with 0.05% Triton-X 100 in 1× PBS (3 min on ice), and blocking with 10% fetal calf serum (FCS) in 1× PBS (1 h). After washing with 1× PBS, the primary antibodies mouse anti-TUBβIII (1 : 2000, Covance) and rabbit anti-TH (1 : 2000, Santa Cruz Biotechnology) were incubated for 90 min at room temperature. After washing with 1× PBS, the secondary antibodies Alexa Fluor 488 Goat Anti-Rabbit and Alexa Fluor 568 Goat Anti-Mouse together with a stain DNA (Hoechst 33342, Invitrogen) were incubated overnight at 4 °C on a rotary shaker. After washing with 1× PBS, confocal images of representative culture chambers were acquired using a confocal microscope (Zeiss LSM 710). After the confocal images were acquired, a spot detection algorithm (Imaris software, Bitplane) was used to detect and count the nuclei in order to be able to calculate the efficiency of differentiation (see the ESI† for more details).

Results

Differentiation of human neuroepithelial stem cells into neurons in microfluidic cell culture

The protocol used to differentiate hNESCs into DNs was successfully implemented in 2-lane and 3-lane OrganoPlates using maintenance and differentiation media as depicted in Fig. 2a. Three hours after loading Matrigel-embedded hNESCs into the OrganoPlate, small cellular aggregates started to form. Cells in these aggregates started to project plasma membrane protrusions (filopodia)[36] to probe their new microenvironment, during perfusion with the maintenance medium and incubation at 37 °C (Fig. 2b). During the days of exposure to the differentiation medium with PMA (day 3 to 10), the morphology of hNESCs was mainly characterised by the extension of those protrusions into more neurite-like structures. In addition to a more defined polarisation (unipolar and bipolar)[37] of the differentiated hNESCs, growth cones and additional filopodia arise from the main neurite[38](ESI† Fig. S1). Furthermore, proliferating and dead hNESCs can be observed in the culture chamber (Fig. 2c). Maturation of differentiating hNESCs into a more robust neuron like phenotype was started by using the differentiation medium without PMA (Fig. 2d). Differentiating neurons were allowed to mature and differentiate for 21 additional days. Throughout this maturation stage, the differentiated neurons had more defined bipolar morphology, growth cones, varicosities and larger neurites, typical of a more mature neuronal phenotype (Fig. 2e) (ESI† Fig. S1).

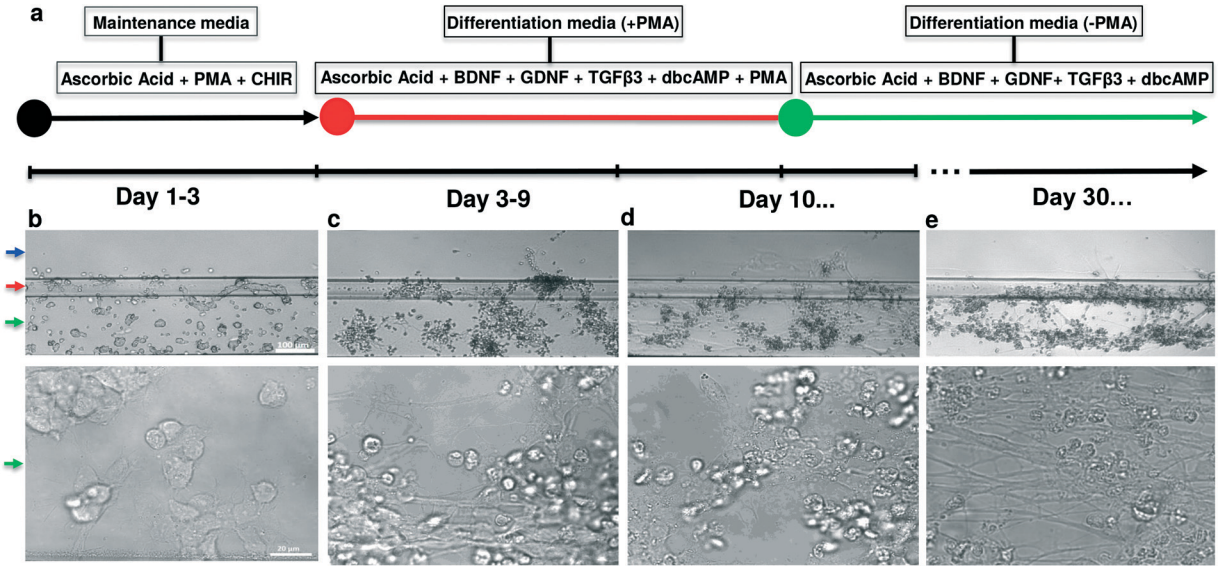

Fig. 2 Differentiation of hNESCs into DNs. (a) Medium components. Bright field images of hNESCs in the 2-lane OrganoPlate: (b) 1 day, (c) 4 days, and (d) 10 days after seeding. (e) hNESCs differentiated into neurons in the 2 lane microfluidic culture chamber after 1 month of differentiation. Scale bars: 100 μm and 20 μm. The blue, red and green arrows on the left indicate the medium lane, phaseguide and culture lane in the OrganoPlate, respectively.

Characterisation of differentiated neurons

2-lane OrganoPlate. In 2-lane bioreactors, differentiated neurons were identified by immunoreactivity for the marker TUBβIII (red, Fig. 3). The staining of differentiated neurons positive for TUBβIII showing the neurite distribution, outreach and ramification in a selected area of the culture lane can be seen in Fig. 3c. Dopaminergic neurons exhibited a spatially homogeneous distribution along the length and breadth of the lane (Fig. 3a). A closer look into the selected area highlighted in Fig. 3a shows the staining of nuclei with Hoechst (blue, Fig. 3b). Differentiated neurons positive for TH confirmed the presence of DNs as shown in Fig. 3d. An enlarged view of the merged image of stained neurons in the selected area of the culture lane is shown in Fig. 3e.

The 2- and 3-lane Organoplates consist of 96 and 40 bioreactors, respectively. Once the hNESCs were loaded to the culture chamber, they had to adapt to the new 3D microenvironment. After 48 hours in culture, approximately 70% of 2- and 3-lane bioreactors had culture chambers with viable cells. A

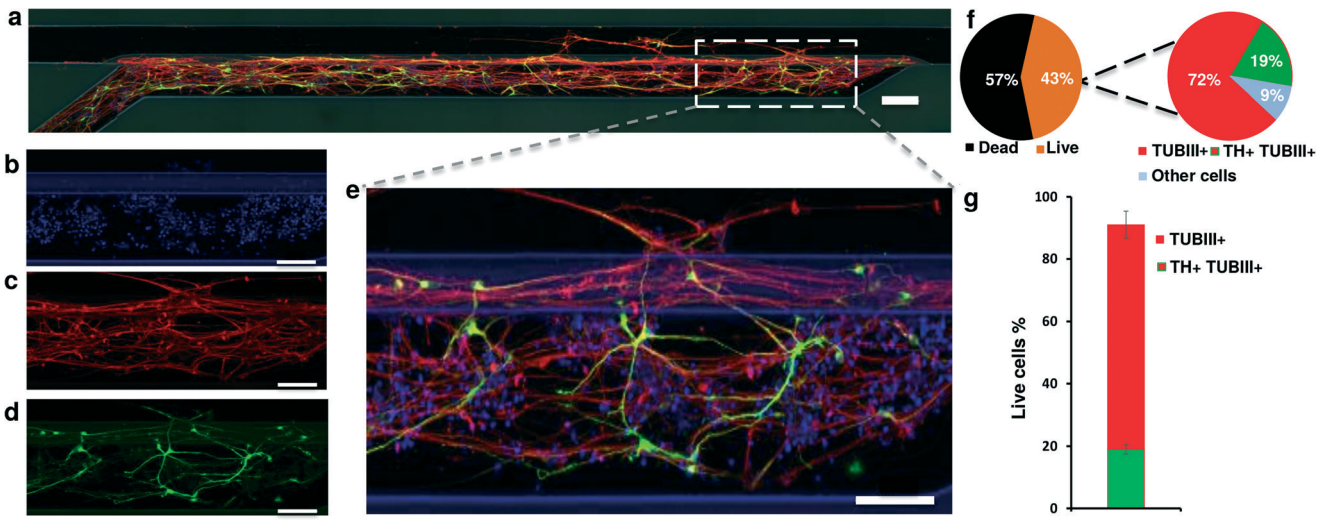

Fig. 3 Differentiation of hNESCs into neurons in a 2-lane microfluidic bioreactor of the OrganoPlate. (a) Immunostaining of differentiated neurons in the 2-lane microfluidic chamber after 1 month of differentiation; scale bar 200 μm. Section of the microfluidic chamber stained for: (b) nuclei with Hoechst in blue, (c) TUBβIII in red, and (d) TH in green; scale bar 50 μm. (e) Merged nuclei, TUBβIII and TH stains; scale bar 100 μm. (f) Efficiency of survival and differentiation of hNESCs into neurons. (g) Efficiency of TH positive neurons (DNs); error bars show the standard deviation from 3 different bioreactors of the 2-lane OrganoPlate.

possible factor contributing to this decrease in bioreactors with viable cells could be the temperature changes experienced by the cells during the sample preparation step, premature gelation of the Matrigel and medium evaporation from wells located at the edge of the plate. In this study, we used cell counts for 3 typical bioreactors in the 2-lane OrganoPlate to calculate the average survival rate in bioreactors with viable cells during the differentiation process. Approximately half of all the cells die in a typical culture lane. Of the live cells, 91% differentiated into TUBβIII positive cells, indicating highly efficient neuronal differentiation (Fig. 3f). 9% of the live cells were negative for both TUBβIII and TH, indicating either a failure to differentiate or differentiation into non-neuronal lineages. Of the live cells, 72% were positive only for TUBβIII and 19% were positive for both TUBβIII and TH (Fig. 3f), indicating efficient differentiation into dopaminergic neurons (Fig. 3g).

3-Lane OrganoPlate. In 3-lane bioreactors, Matrigel-embedded cells were flanked by two medium perfusion lanes. A homogeneous distribution of differentiated neurons was observed throughout the length and breadth of typical culture lanes (Fig. 4a). Similar to Fig. 3b, the spatial distribution of cell nuclei (Hoechst staining) in a selected area of the culture lane is illustrated in Fig. 4b, neurites (TUBβIII staining) in Fig. 4c, and neurons positive for TH in Fig. 4d; an enlarged view of the selected area in the culture lane showing the merged distribution of used cellular markers of differentiated neurons is shown in Fig. 4e.

In the cell culture lanes of the 3-lane OrganoPlate, 65% of the cells died during the differentiation process. Out of the 35% surviving cells, 11% were negative for TUBβIII and TH (undifferentiated remaining neural stem cells). Among the remaining 89% of cells differentiated into neurons, 78% were only positive for TUBβIII and 11% were positive for TUBβIII and TH as shown in Fig. 4f. The efficiency of TH positive neuronal differentiation in the bioreactors of the 3-lane OrganoPlate was therefore 11% (Fig. 4g).

3D distribution of differentiated dopaminergic neurons

A 3D reconstruction of the differentiated neurons in a representative culture chamber of the 2-lane OrganoPlate revealed the distribution of differentiated neurons positive for TUBβIII and TH (Fig. 5a). Both medium perfusion and cell culture lanes can be seen, separated by a phaseguide, demonstrating that cells are confined to the culture lane. A longitudinal view along the same culture lane revealed that many cells had migrated toward the top of the Matrigel (Fig. 5b). Furthermore the upper surface of the Matrigel no longer reached the top of the culture lane, rather it had contracted to create an apparently concave upper surface. A side view of the same culture lane shows the spatial localisation of neurite projections relative to the height of the channel (Fig. 5c). The top side view orientation of the differentiated cells in the channels shows the level of connectivity among TUBβIII and TH positive neurons (Fig. 5d).

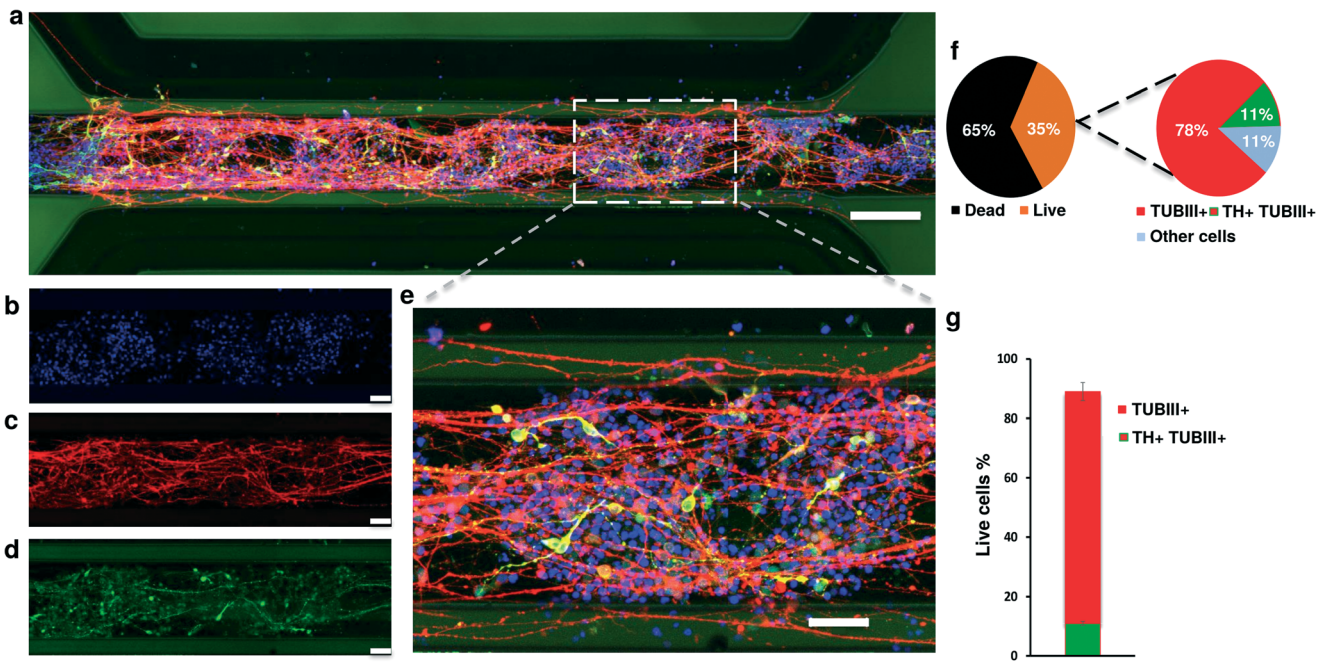

Fig. 4 Differentiation of hNESCs into neurons in a 3-lane microfluidic bioreactor of the OrganoPlate. (a) Immunostaining of differentiated neurons in the 3-lane microfluidic chamber after 1 month of differentiation; scale bar 200 μm. Section of the microfluidic chamber stained for: (b) nuclei with Hoechst, (c) TUBβIII, and (d) TH; scale bar 50 μm. (e) Merged nuclei, TUBβIII and TH stains; scale bar is 100 μm. (f) Correlation of live–dead cells regarding differentiation of hNESCs into neurons and efficiency of differentiation. (g) Efficiency of TH positive (mDN) neurons; error bars show the standard deviation from 3 different bioreactors of the 3 lane OrganoPlate.

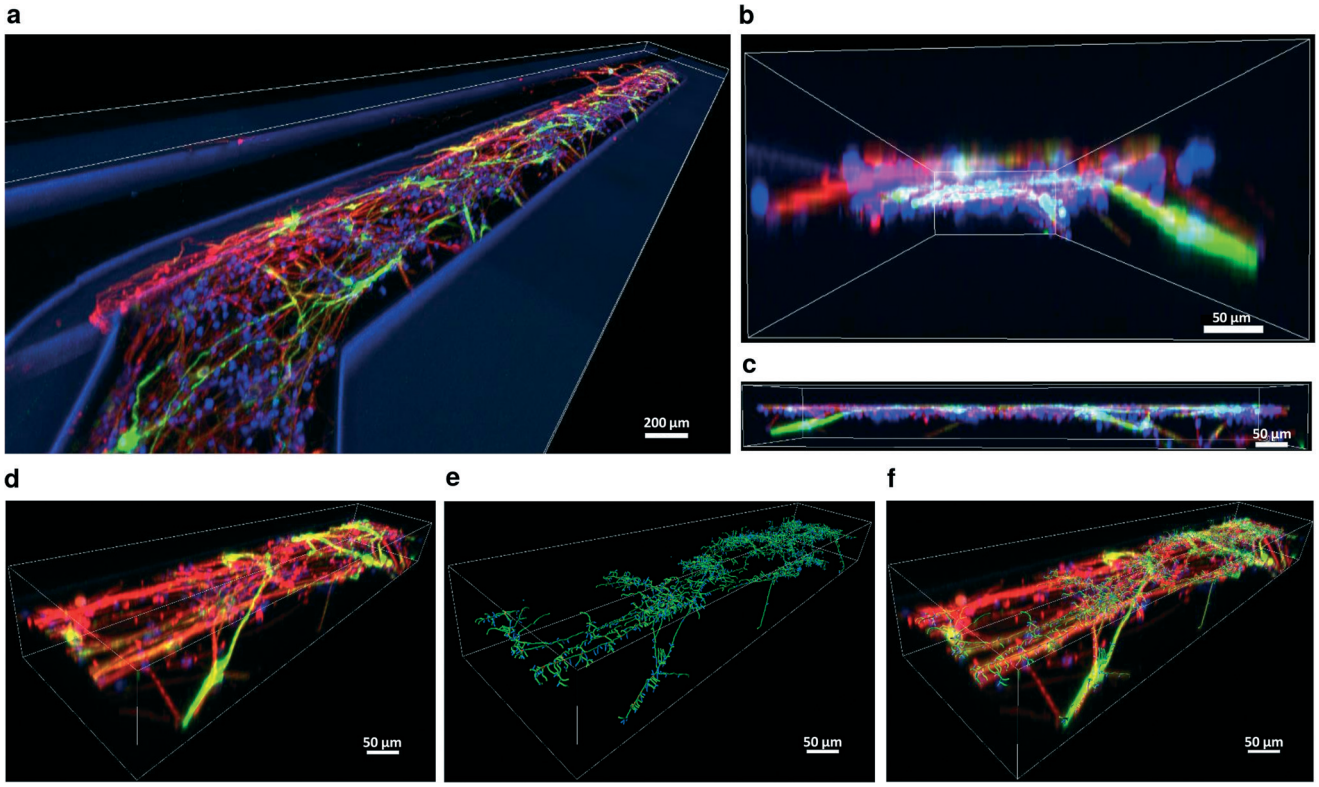

Fig. 5 3D representation and distribution of TH positive differentiated neurons in the 2-lane microfluidic culture chamber of the OrganoPlate. (a) Top view of the entire culture chamber; scale bar 200 μm. (b) Inside view and (c) side view of a selected area of the culture lane; scale bar 50 μm. (d) Top view of the selected area, (e) reconstruction of neuronal filaments of TH and TUBβIII-positive neurons in the selected area, and (f) overlap of (d) and (e); scale bar 50 μm.

Surface reconstruction and filament tracing revealed a truly three-dimensional distribution of differentiated cells in the culture lane, as shown in Fig. 5e and ESI† movie 2. An overlay of the neuronal distribution and the filament reconstruction of neurons located in this area of the plate shows the high level of branching, interconnectivity and the length of neurites of differentiated neurons (Fig. 5f).

Electrophysiological activity of differentiated neurons

Analysis of calcium imaging time-series of representative culture chambers revealed spontaneous neuronal activity in several differentiated neurons. A calcium transient, evoked by an action potential, is characterised by a fast rise in intracellular calcium concentration due to neuronal depolarisation followed by a slower exponential decay corresponding to the slow unbinding rate of calcium ions from the fluorescent probe.[39,40] Fig. 6 shows the somatic fluorescence signals extracted from spontaneously active neurons in the 3-lane OrganoPlate, where calcium transients evoked by action potentials were visible (see also ESI† movie 3).

Fig. 6a depicts the mean fluorescence image of a TH immunoreactive differentiated neuron. Using the Fluo-4 fluorescence trace of this neuron, we applied the algorithm reported by Vogelstein *et al.*[33] to infer the most probable spike train underlying the trace (Fig. 6b). Interestingly, the resulting spontaneous calcium transients and the underlying spikes tend to be regular and this is consistent with previous *in vitro* studies on the tonic electrophysiological activity of DNs.[41,42] Fig. 6c–e illustrate the fluorescence traces and inferred spike trains from three different TH-negative neurons. These results show that TH-negative neurons tend to depolarise in more irregular temporal patterns than TH-positive cells. Fig. 7 shows the calcium signals extracted from the soma, neurite and neurite terminal of a typical electrophysiologically active neuron in the culture chamber of the 2-lane OrganoPlate. At our sampling rate of 8.4 Hz, calcium transients appeared to be synchronised between these three regions, indicating that each action potential does propagate along neurites.

Discussion

The degeneration of substantia nigra dopaminergic neurons is one of the hallmarks of Parkinson's disease.[43] The efficient generation of iPSC-derived dopaminergic neuronal *in vitro* cultures with phenotypic properties proximal to those observed *in vivo* in patients and matched controls is therefore an important goal for personalised biomedicine approaches to Parkinson's disease. We successfully differentiated human neuroepithelial stem cells (hNESCs) into dopaminergic neurons within established microfluidic cell culture bioreactors.[26]

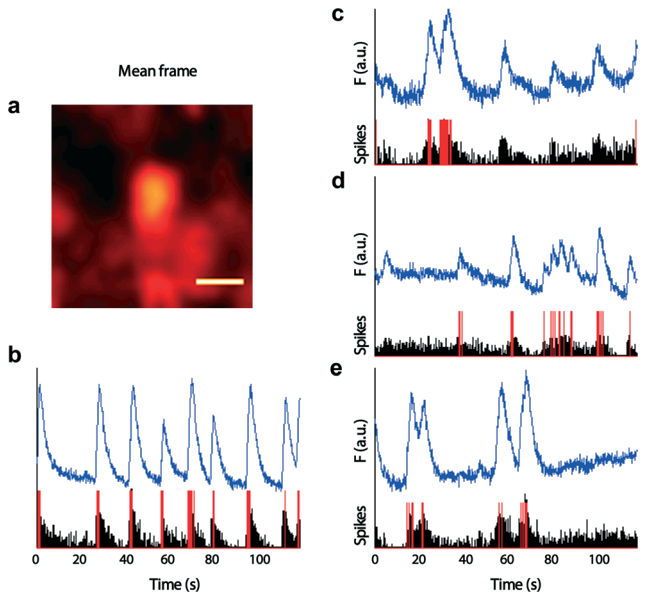

Fig. 6 Monitoring of spontaneous neuronal activity of differentiated neurons in the culture chamber of the 3-lane OrganoPlate. (a) Mean frame of a field of view representing an electrophysiologically active TH immunoreactive neuron; scale bar 20 μm. (b) Fluorescence trace (blue line) and the inferred spike train corresponding to the neuron in (a) (black bars using the fast non-negative deconvolution filter and red bars after thresholding). (c–e) Fluorescence traces corresponding to three different non-TH positive neurons and the underlying spike trains.

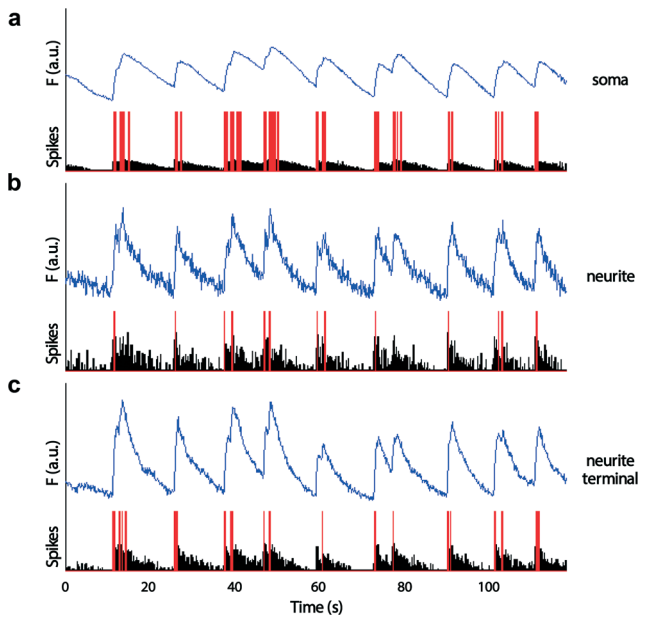

Fig. 7 Fluorescence traces (blue lines) and the inferred spike trains corresponding to different regions of a differentiated neuron in the culture chamber of the 2-lane OrganoPlate (black bars using the fast non-negative deconvolution filter and red bars after thresholding): (a) soma, (b) neurite, and (c) neurite terminal.

In each bioreactor, a 3D lane of Matrigel-embedded cells is flanked by bulk flow of fluid medium on one or both sides. Human neuroepithelial stem cells (hNESCs) were derived from iPSCs using an established macroscopic cell culture protocol that only requires small molecules.[13] Differentiation of hNESCs into midbrain-specific dopaminergic neurons requires the use of expensive reagents. Our use of these reagents in microfluidic cell culture is approximately 10 times less than in macroscopic culture, making microfluidic culture more economical.

The calculation of the percentage of dead cells in the culture is based on counting the nuclei (Hoechst stain) in the culture lane. The percentage of dead cells reflects the prevalence of cell death after a 30 day culture period, because dead gel-embedded cells are not flushed out by renewal of media. This is in contrast to two dimensional macroscopic culture where one typically measures the incidence of cell death between medium renewals, each of which flushes away dead cells that detach from the underlying culture surface. Differentiation efficiency has been observed to increase in a sigmoidal fashion with time.[13] After a 30 day exposure to differentiation media, we achieved an immunocytologically confirmed neuronal differentiation efficiency of 91%, which compares favourably with the 50% efficiency observed in macroscopic culture after 21 days.[13] The remaining cells (TUBβIII negative, TH negative) are either undifferentiated hNESCs or astrocytes as observed in macroscopic culture and as suggested by phase contrast images indicating an astrocytic morphology (data not shown). Of the immunocytologically confirmed neurons, the dopaminergic neuronal differentiation efficiency was 19% and 11% within the 2- and 3-lane microfluidic bioreactors, respectively, as compared to the 30% efficiency observed in macroscopic culture after 21 days.[13] Gel-embedded cells in a 3-lane bioreactor are flanked by medium perfusion on two sides, as opposed to one side in a 2-lane bioreactor. The lower differentiation efficiency in 3-lane bioreactors may be due to increased dilution of paracrine factors suggesting that modulation of the medium perfusion rate could lead to higher differentiation efficiency.

In mouse[41] and guinea pig[42] brain slices, nigrostriatal dopaminergic neurons exhibit spontaneous firing, at a highly regular rate. Our calcium imaging, performed *in situ*, confirmed the spontaneous electrophysiological activity in differentiated neurons, with action potentials propagating along neurites. A more regular firing pattern was observed in dopaminergic neurons (TUBβIII and TH positive cells) as opposed to other neurons (TUBβIII positive, TH negative) indicating that these cells are electrophysiologically more proximal to nigrostriatal dopaminergic neurons *in vivo*. We employed a deconvolution algorithm[33] to infer the probability of a depolarisation event underlying successive intervals of the calcium signal. Patch clamp recordings, in parallel to calcium imaging from individual hNESC-derived dopaminergic neurons, would be required to tune the free parameters of the deconvolution algorithm and express greater confidence in the predicted depolarisation events since nigrostriatal dopaminergic neurons are known to exhibit atypically broad action potentials.[44]

Our results reinforce the previously observed biocompatibility of the materials used in our phase-guided 3D cell culture bioreactors (OrganoPlate, Mimetas BV). This is important because assays of biocompatibility must be completed with a range of cell types as different cell types do respond differently to the same cell culture device.[45] This is especially so with microfluidic cell culture, where the ratio between cellular volume and culture device surface area (in diffusive contact with cells) is typically much lower than for macroscopic culture.[46] We use a phaseguide to separate the medium and culture lanes, measuring 1/4 of the height of the lane; therefore at least 3/4 of the surface area of the gel in the culture lane is in diffusive contact with fresh media. This provides ample supply of fresh nutrients and dissolved gasses and avoids any requirement for microfabricated pillar arrays or other barriers to nutrient exchange.

Reinhardt *et al.*[13] used Matrigel to coat the surface of macroscopic culture plates in which hNESCs were cultured. In contrast, we first mixed hNESCs with fluid Matrigel at 4 °C, and then dispensed this mixture from a pipette into a cooled bioreactor. This mixture gelates when the temperature of the bioreactor rises above 10 °C. This loading step requires careful control over temperature to ensure that the mixture remains fluid until lane loading is complete. We have observed that premature gelation lowers cell viability. This may be due to increased viscosity of the partially gelated mixture which would result in sheer stress to embedded cells during loading. After gelation, hNESCs should have an isotropic cellular morphology with any anisotropy indicative of sheer stress during loading. Regarding the ratio of live : dead cells, it is hard to obtain comparable data from macroscopic 2D culture where dead cells detach and are flushed away by medium replacement. In contrast, dead cells continue to reside *in situ* in our 3D culture.

While maintaining the Matrigel at 4 °C keeps it fluid, 37 °C is the optimal temperature for culture of most human cells. Mixing hNESCs with fluid Matrigel at 4 °C does expose them to a cold shock[47] which must be as long as the loading of all desired bioreactors on a single microfluidic plate. Of the microfluidic bioreactors loaded with hNESCs, approximately 7 out of 10 culture chambers had aggregates of viable cells after 48 h in culture. It may be that the cold shock experienced by the hNESCs contributes to the collective loss of viability in non-viable chambers, though some loss of collective viability is also normally expected amongst any set of macroscopic culture wells. Future experiments are required with alternatives to Matrigel that can suspend cells in fluid during loading and gelate in a controlled manner without harming embedded cells yet act as a biocompatible extracellular matrix upon gelation.

Conclusions

We successfully differentiated human neuroepithelial stem cells into dopaminergic neurons within phase-guided, three dimensional microfluidic cell culture bioreactors. After 30 days of differentiation, *in situ* morphological, immunocytological and electrophysiological characterisation of dopaminergic neurons confirmed the biological fidelity of this new *in vitro* model and emphasised the biocompatibility of this phase-guided microfluidic device.

Each microfluidic bioreactor requires a fraction of the expensive reagents typically used for macroscopic culture and our arrays of microfluidic bioreactors are arranged in a microtiter plate format that is compatible with standard laboratory automation. These features, combined with the establishment of biobanks of patient-derived induced pluripotent stem cells, provide an efficient route to personalise industrial-scale drug discovery.

Acknowledgements

The authors thank Inga Werthschulte for the technical support in providing the hNESCs used in all experiments. The AFR (Aides à la Formation-Recherche) Training allowance granted to Edinson Lucumi Moreno by FNR (Fonds National de la Recherche Luxembourg) is also acknowledged. A Pelican award from the Fondation du Pelican de Mie et Pierre Hippert-Faber supported K. H. The JCS lab is supported by a CORE grant from the Fonds National de la Recherche.

References

1 F. Ali, S. R. W. Stott and R. A. Barker, *Exp. Neurol.*, 2014, **260**, 3–11.
2 J. Yu, M. A. Vodyanik, K. Smuga-Otto, J. Antosiewicz-Bourget, J. L. Frane, S. Tian, J. Nie, G. A. Jonsdottir, V. Ruotti, R. Stewart, I. I. Slukvin and J. A. Thomson, *Science*, 2007, **318**, 1917–1920.
3 K. Takahashi, K. Tanabe, M. Ohnuki, M. Narita, T. Ichisaka, K. Tomoda and S. Yamanaka, *Cell*, 2007, **131**, 861–872.
4 M. Bellin, M. C. Marchetto, F. H. Gage and C. L. Mummery, *Nat. Rev. Mol. Cell Biol.*, 2012, **13**, 713–726.
5 R. Gonzalez, I. Garitaonandia, T. Abramihina, G. K. Wambua, A. Ostrowska, M. Brock, A. Noskov, F. S. Boscolo, J. S. Craw, L. C. Laurent, E. Y. Snyder and R. A. Semechkin, *Sci. Rep.*, 2013, **3**, 1463.
6 J. N. L. Grand, L. Gonzalez-Cano, M. A. Pavlou and J. C. Schwamborn, *Cell. Mol. Life Sci.*, 2014, 1–25.
7 A. Swistowski, J. Peng, Q. Liu, P. Mali, M. S. Rao, L. Cheng and X. Zeng, *Stem Cells*, 2010, **28**, 1893–1904.
8 S. M. Chambers, C. A. Fasano, E. P. Papapetrou, M. Tomishima, M. Sadelain and L. Studer, *Nat. Biotechnol.*, 2009, **27**, 275–280.
9 H. Braak and K. Del Tredici, *Adv. Anat., Embryol. Cell Biol.*, 2009, **201**, 1–119.
10 H. N. Nguyen, B. Byers, B. Cord, A. Shcheglovitov, J. Byrne, P. Gujar, K. Kee, B. Schüle, R. E. Dolmetsch, W. Langston, T. D. Palmer and R. R. Pera, *Cell Stem Cell*, 2011, **8**, 267–280.
11 A. Sanchez-Danes, Y. Richaud-Patin, I. Carballo-Carbajal, S. Jimenez-Delgado, C. Caig, S. Mora, C. Di Guglielmo, M. Ezquerra, B. Patel, A. Giralt, J. M. Canals, M. Memo, J.

Alberch, J. Lopez-Barneo, M. Vila, A. M. Cuervo, E. Tolosa, A. Consiglio and A. Raya, *EMBO Mol. Med.*, 2012, **4**, 380–395.
12 O. Cooper, H. Seo, S. Andrabi, C. Guardia-Laguarta, J. Graziotto, M. Sundberg, J. R. McLean, L. Carrillo-Reid, Z. Xie, T. Osborn, G. Hargus, M. Deleidi, T. Lawson, H. Bogetofte, E. Perez-Torres, L. Clark, C. Moskowitz, J. Mazzulli, L. Chen, L. Volpicelli-Daley, N. Romero, H. Jiang, R. J. Uitti, Z. Huang, G. Opala, L. A. Scarffe, V. L. Dawson, C. Klein, J. Feng, O. A. Ross, J. Q. Trojanowski, V. M.-Y. Lee, K. Marder, D. J. Surmeier, Z. K. Wszolek, S. Przedborski, D. Krainc, T. M. Dawson and O. Isacson, *Sci. Transl. Med.*, 2012, **4**, 141ra90.
13 P. Reinhardt, M. Glatza, K. Hemmer, Y. Tsytsyura, C. S. Thiel, S. Honing, S. Moritz, J. A. Parga, L. Wagner and J. M. Bruder, *et al.*, *PLoS One*, 2013, **8**, e59252.
14 J. W. Haycock, in *3D Cell Culture*, ed. J. W. Haycock, Humana Press, 2011, pp. 1–15.
15 A. L. Paguirigan and D. J. Beebe, *BioEssays*, 2008, **30**, 811.
16 S. Halldorsson, E. Lucumi, R. Gómez-Sjöberg and R. M. T. Fleming, *Biosens. Bioelectron.*, 2015, **63C**, 218–231.
17 G. Hargus, O. Cooper, M. Deleidi, A. Levy, K. Lee, E. Marlow, A. Yow, F. Soldner, D. Hockemeyer, P. J. Hallett, T. Osborn, R. Jaenisch and O. Isacson, *Proc. Natl. Acad. Sci. U. S. A.*, 2010, **107**, 15921–15926.
18 K. Hemmer, M. Zhang, T. van Wüllen, M. Sakalem, N. Tapia, A. Baumuratov, C. Kaltschmidt, B. Kaltschmidt, H. R. Schöler, W. Zhang and J. C. Schwamborn, *Stem Cell Rep.*, 2014, **3**, 423–431.
19 G. Hargus, *et al.*, *Cell Rep.*, 2014, **8**, 1697–1703.
20 C. Brito, D. Simão, I. Costa, R. Malpique, C. I. Pereira, P. Fernandes, M. Serra, S. C. Schwarz, J. Schwarz, E. J. Kremer and P. M. Alves, *Methods*, 2012, **56**, 452–460.
21 E. J. Gualda, D. Simao, C. Pinto, P. M. Alves and C. Brito, *Front. Cell. Neurosci.*, 2014, **8**, 221.
22 D. van Noort, S. M. Ong, C. Zhang, S. Zhang, T. Arooz and H. Yu, *Biotechnol. Prog.*, 2009, **25**, 52–60.
23 D. Huh, H. J. Kim, J. P. Fraser, D. E. Shea, M. Khan, A. Bahinski, G. A. Hamilton and D. E. Ingber, *Nat. Protoc.*, 2013, **8**, 2135–2157.
24 J. H. Sung, M. B. Esch, J.-M. Prot, C. J. Long, A. Smith, J. J. Hickman and M. L. Shuler, *Lab Chip*, 2013, **13**, 1201–1212.
25 S. N. Bhatia and D. E. Ingber, *Nat. Biotechnol.*, 2014, **32**, 760–772.
26 S. J. Trietsch, G. D. Israëls, J. Joore, T. Hankemeier and P. Vulto, *Lab Chip*, 2013, **13**, 3548–3554.
27 P. Vulto, S. Podszun, P. Meyer, C. Hermann, A. Manz and G. A. Urban, *Lab Chip*, 2011, **11**, 1596–1602.
28 E. Yildirim, S. J. Trietsch, J. Joore, A. v. d. Berg, T. Hankemeier and P. Vulto, *Lab Chip*, 2014, **14**, 3334–3340.
29 J. Lee, M. J. Cuddihy and N. A. Kotov, *Tissue Eng., Part B*, 2008, **14**, 61–86.
30 M. W. Tibbitt and K. S. Anseth, *Biotechnol. Bioeng.*, 2009, **103**, 655–663.
31 H. K. Kleinman and G. R. Martin, *Semin. Cancer Biol.*, 2005, **15**, 378–386.
32 N. Stuurman, A. D. Edelstein, N. Amodaj, K. H. Hoover and R. D. Vale, *Curr. Protoc. Mol. Biol.*, 2010, **92**, 14.20.2–14.20.17.
33 J. T. Vogelstein, A. M. Packer, T. A. Machado, T. Sippy, B. Babadi, R. Yuste and L. Paninski, *J. Neurophysiol.*, 2010, **104**, 3691–3704.
34 M. M. Daadi, B. A. Grueter, R. C. Malenka, D. E. Redmond and G. K. Steinberg, *PLoS One*, 2012, **7**, e41120.
35 Y. Yan, D. Yang, E. D. Zarnowska, Z. Du, B. Werbel, C. Valliere, R. A. Pearce, J. A. Thomson and S.-C. Zhang, *Stem Cells*, 2005, **23**, 781–790.
36 P. K. Mattila and P. Lappalainen, *Nat. Rev. Mol. Cell Biol.*, 2008, **9**, 446–454.
37 S. Iden and J. G. Collard, *Nat. Rev. Mol. Cell Biol.*, 2008, **9**, 846–859.
38 A. J. Koleske, *Nat. Rev. Neurosci.*, 2013, **14**, 536–550.
39 C. Stosiek, O. Garaschuk, K. Holthoff and A. Konnerth, *Proc. Natl. Acad. Sci. U. S. A.*, 2003, **100**, 7319–7324.
40 H. C. Johannssen and F. Helmchen, *J. Physiol.*, 2010, **588**, 3397–3402.
41 M. K. Sanghera, M. E. Trulson and D. C. German, *Neuroscience*, 1984, **12**, 793–801.
42 W. H. Yung, M. A. Häusser and J. J. Jack, *J Physiol*, 1991, **436**, 643–667.
43 P. M. A. Antony, N. J. Diederich, R. Krüger and R. Balling, *FEBS J.*, 2013, **280**, 5981–5993.
44 A. A. Grace and B. S. Bunney, *J. Neurosci.*, 1984, **4**, 2866–2876.
45 P. M. van Midwoud, A. Janse, M. T. Merema, G. M. M. Groothuis and E. Verpoorte, *Anal. Chem.*, 2012, **84**, 3938–3944.
46 A. L. Paguirigan and D. J. Beebe, *Integr. Biol.*, 2009, **1**, 182–195.
47 M. F. Underhill and C. M. Smales, *Cytotechnology*, 2007, **53**, 47–53.

